China Geology 7 (2024) 686−701

China Geology

Journal homepage: http://chinageology.cgs.cn
https://www.sciencedirect.com/journal/china-geology

Multi-stage formation of the Feragen ophiolite, Norway: Implication from petrology and geochemistry of peridotites and chromitites and its potential for prospecting

Tian Qiu[a, b], Fa-hui Xiong[a, b, c,*], David G. Gee[d], Yuan Li[a], Jing-sui Yang[a, b, e]

[a] *Center for Advanced Research on the Mantle (CARMA), Key Laboratory of Deep-Earth Dynamics of Ministry of Natural Resources, Institute of Geology, Chinese Academy of Geological Sciences, Beijing* 100037, *China*
[b] *Southern Marine Science and Engineering Guangdong Laboratory, Guangzhou* 511458, *China*
[c] *Key Laboratory of Depositional Mineralization and Sedimentary Minerals, Shandong University of Science and Technology, Qingdao* 266590, *China*
[d] *Orogen Dynamics Department of Earth Sciences Uppsala University Villavagen* 16, *Uppsala SE*-75236, *Sweden*
[e] *School of Earth Sciences and Engineering, Nanjing University, Nanjing* 210023, *China*

ARTICLE INFO

Article history:
Received 19 December 2022
Received in revised form 20 March 2023
Accepted 10 April 2023
Available online 12 June 2023

Keywords:
Geochemistry
fO_2
Platinum-group elements
High-Cr podiform chromitites
SSZ peridotite
Harzburgites
Feragen ophiolite
Norway
Dunite
Abyssal peridotite

ABSTRACT

The ultramafic massif of Feragen, which belongs to the eastern ophiolitic belt of Norway, has abundant amounts of chromite ores. Recent studies have revealed a complex melt evolution in a supra-subduction zone (SSZ) environment. This study presents new whole-rock major element, trace element, and platinum-group element chemistry to evaluate their petrogenesis and tectonic evolution. Harzburgites have high CaO, Al_2O_3, TiO_2, MgO, and REE contents corresponding to abyssal peridotites, whereas dunites have low CaO, Al_2O_3, TiO_2, MgO, and REE contents corresponding to SSZ peridotites. The Cr# and TiO_2 of chromian spinels in the harzburgites suggest as much as about 15%–20% melting and the dunites are more depleted with > 40% melting. The harzburgites and the dunites and high-Cr chromitites represent, respectively, the products of low-degree partial melting in a back-arc setting, and the products of melt-rock interaction in a SSZ environment. The calculated fO_2 values for dunites and high-Cr chromitites (−0.17 – +0.23 and +2.78 – +5.65, respectively and generally above the FMQ buffer) are also consistent with the interaction between back-arc ophiolites with oxidized boninitic melts in a SSZ setting.

1. Introduction

Ophiolites are fragments of upper mantle and oceanic crust which record the tectonic evolution of ocean basins from their rift-drift and spreading stages to subduction initiation and final closure (Moores EM, 1982; Dilek Y and Robinson PT, 2003; Dilek Y and Furnes H, 2011, 2014; Uysal I et al., 2015). Petrographic and geochemical studies of upper mantle peridotites specifically, the critical mineral phases (such as chromian spinel, olivine, clinopyroxene, and orthopyroxene) in mantle peridotites are considered as clues of melt generation and mantle-melt interaction, and ultimately the tectonic settings of ophiolite formation (Pearce JA et al., 2000; Niu Y, 2004; Zhou MF et al., 2005; Arai S et al., 2006; Uysal I et al., 2015). Chromitites, occurring usually in the upper-mantle part of the ophiolite pseudo-section are economically important as source of chromium, and scientifically important because they encapsulate information on the nature of ancient upper mantle, young oceanic mantle, processes of melt formation and percolation in the mantle (Ahmed A and Arai S, 2002; Gervilla F et al., 2005; Rollinson H, 2008; Page P and Barnes SJ, 2009; Borisova A et al., 2012). A general agreement has emerged that chromitites form in depleted mantle sections of ophiolites from supra-subduction zone (SSZ) environments due to melt–rock reaction (Arai S and Yurimoto H, 1994; Zhou MF et al., 1994, 1998, 2014; Ballhaus C, 1998; Melcher F et al., 1999; Uysal I et al., 2005, 2007; Xiong FH et al., 2015). Peridotites and podiform chromitites in ophiolites reflect multi-stage processes involving subduction of lithospheric slabs into the transition zone, crystallization of some massive chromitites at depth, incorporation of UHP and highly reduced phases into the chromitites and entrapment of oceanic lithospheric slabs above subduction zones where they interact with subduction-

First author: *E-mail address*: qiutian2010@126.com (Tian Qiu).

* Corresponding author: *E-mail address*: xiongfahui@126.com (Fa-hui Xiong).

Literary editor: Xi-jie Chen
doi:10.31035/cg2023017
2096-5192/© 2024 China Geology Editorial Office.

related melts (Yamamoto S et al., 2009; Yang JS et al., 2013, 2014; Robinson PT et al., 2015; Xiong FH et al., 2015, 2022; Li JQ et al., 2023). Moreover, many ophiolites, proposed to have formed in SSZ settings, are considered to have been underwent a sequence of events in response to changes in the tectonic setting from mid-ocean ridges to subduction zones (Beccaluva I et al., 1984, 1994; Pearce JA et al., 1984; Shervais JW, 2001).

A large number of ultramafic bodies are found in the southern part of the Trondheim basin, which crop out between Feragen in the east and Otta in the west, Norway. Previous studies considered that these ultramafic bodies were formed by cumulate processes in a back-arc environment prior to tectonic emplacement during the orogensis which produced the Trondheim nappe (Moore AC and Hultin I, 1980). However, our recent studies on the eastern ultramafic body, known as the Feragen ophiolite, has revealed a complex melt evolution in a supra-subduction zone environment. In this study, we present detailed mineralogical and geochemical data on the studied peridotites and chromitites of the Feragen ophiolite, to constrain the tectonic settings of its formation and provide a testable hypothesis for its tectono-magmatic evolution.

2. Geology of the Feragen Ophiolite

The Feragen ophiolite crops out over an area of about 15 km^2 in Sør-Trøndelag, east- central Norway (Fig. 1). It is one of several ultramafic bodies occurring along the southern and eastern margins of the Trondheim Nappe Complex and regarded as typical of "alpine-type" peridotite situated within gneissic Cambrian–Silurian sequences (Moore AC and Hultin I, 1980; Nilsson LP et al., 1997, 2005). The ophiolite consists chiefly of harzburgite, dunite, and minor chromitites with various degrees of serpentinization. Limited occurrences of Mg-carbonates (magnesite, nesquehonite) which formed during weathering have been reported along fractures of the Feragen peridotites close to the contact with the country rocks (Moore AC and Hultin I, 1980; Beinlich A and Austrheim H, 2012; Ulven IO et al., 2017; Dunkel KG et al., 2019).

The northern contact between the serpentinized ultramafic rocks and the country rocks is covered by Devonian serpentine conglomerate similar to what has been described

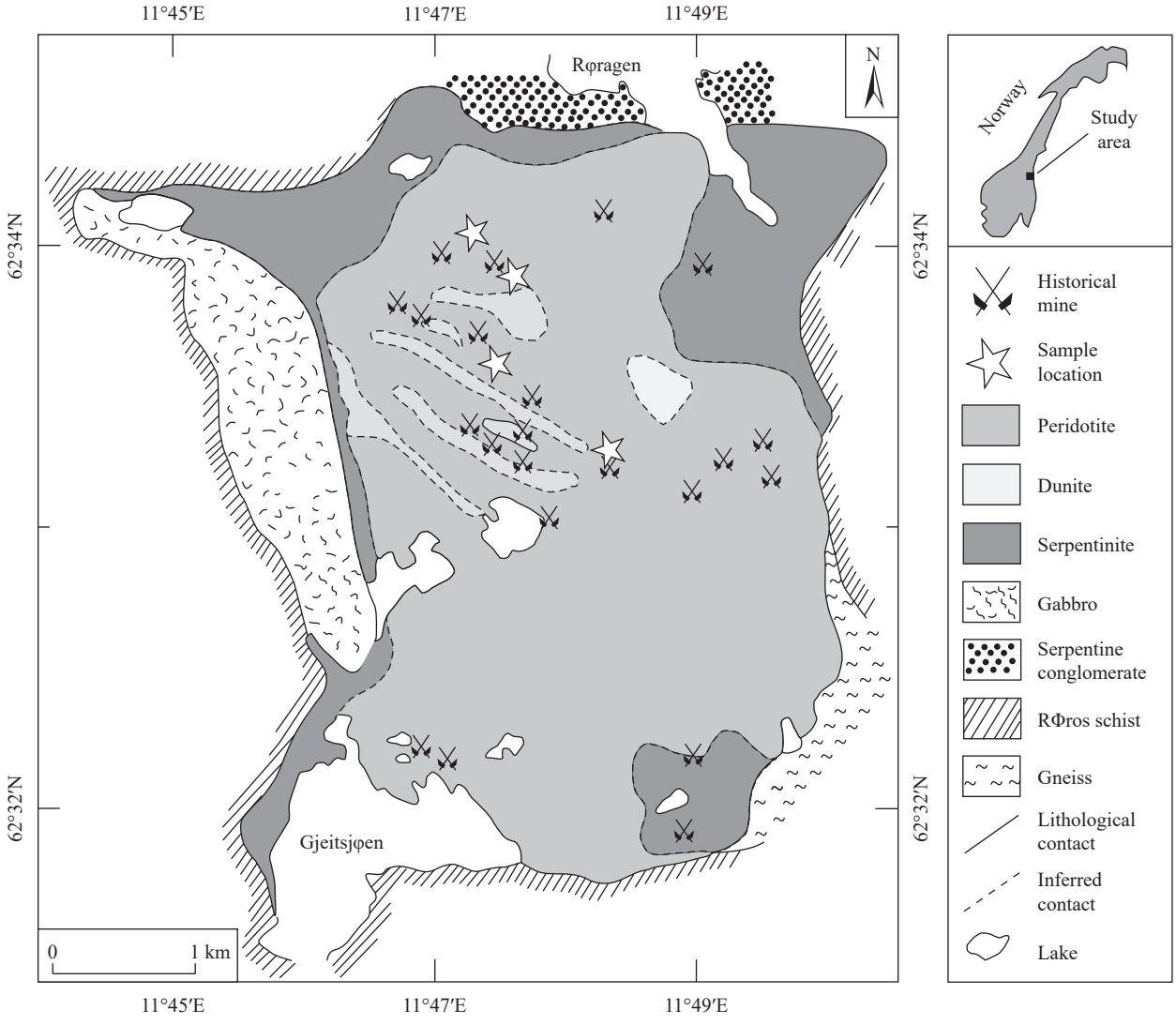

Fig. 1. Simplified tectonostratigraphic map of the Feragen ophiolite, Norway (modified from Moore AC and Hultin I, 1980).

previously in other the Devonian sedimentary basins along the western coast of southern Norway (Fig. 1; Roberts D, 1974; Nilsson LP and Roberts D, 2014; Beinlich A et al., 2018). Precambrian gneiss borders the Feragen ophiolite in the southeast and gabbro in the west (Moore AC and Hultin I, 1980). The Feragen ophiolite has been mined extensively for chromite and was the most important source of chrome in Norway until mining ceased around 1927. Several hundred small open pits and about 20 shafts were operated for open-pit and underground mining, respectively.

3. Field occurrence and petrography

3.1. Harzburgites

Most harzburgites are massive and dark yellow in color (Figs. 2a−b). Both serpentinite and tectonic breccias are locally present in the harzburgites (Fig. 2b). Harzburgites, most of which are coarse-grained with granular textures, consist mainly of olivine (60−75 vol%) and orthopyroxene (20−35 vol%) with minor clinopyroxene (< 5 vol%) and chromian spinel (Fig. 3a).

Olivine occurs generally as large granular crystals (0.1−0.3 mm), showing notable deformation features, such as deformation lamellae, kink banding and wavy extinction. Some olivine grains occur as small inclusions in both orthopyroxene and chromian spinel. Narrow shear bands, marked by recrystallized, fine-grained olivine are commonly observed in harzburgite samples. Orthopyroxenes mostly form large, euhedral to subhedral grains (0.5−1 mm) in harzburgite (Fig. 3a), showing extensive crystal flexural bends, undulatory extinction and gliding twins. Clinopyroxenes occur as irregular interstitial grains between olivine and orthopyroxene in the harzburgites. Chromian spinels are small and interstitial grains scattered in the harzburgite (Fig. 3a). Some grains occur as euhedral inclusions in olivine and orthopyroxene.

3.2. Dunites

Dunites occur commonly as lenses or veins in harzburgites with brownish-black in color (Figs. 2b–c). Most dunites are serpentinized and consist chiefly of olivine (90−95 vol%), serpentine (>5 vol%) and minor orthopyroxene (<1 vol%) with traces of chromian spinel and magnetite (Fig. 3b). Olivine grains are mostly 0.1−0.5 mm in diameter, and some of them are characterized by fine-grained and mosaic texture. Olivine has been partly altered by serpentine along cracks and grain boundaries, leading eventually to small "islands" of relict olivine (Fig. 3b). Orthopyroxene occurring as pseudomorphism has been mostly altered by serpentine and chlorite. Chromian spinels are commonly scattered in the dunites but locally they are sufficiently concentrated to form disseminated chromitites (Figs. 3b-c). The chromian spinel grains are euhedral to subhedral and some of which was altered by magnetite along rims.

3.3. Chromitites

Podiform chromitites are predominantly disseminated type and scattered through the harzburgites of the Feragen ophiolite (Fig. 2d). Chromian spinels in the chromite ore bodies are generally euhedral to subhedral in habit (Fig. 3c).

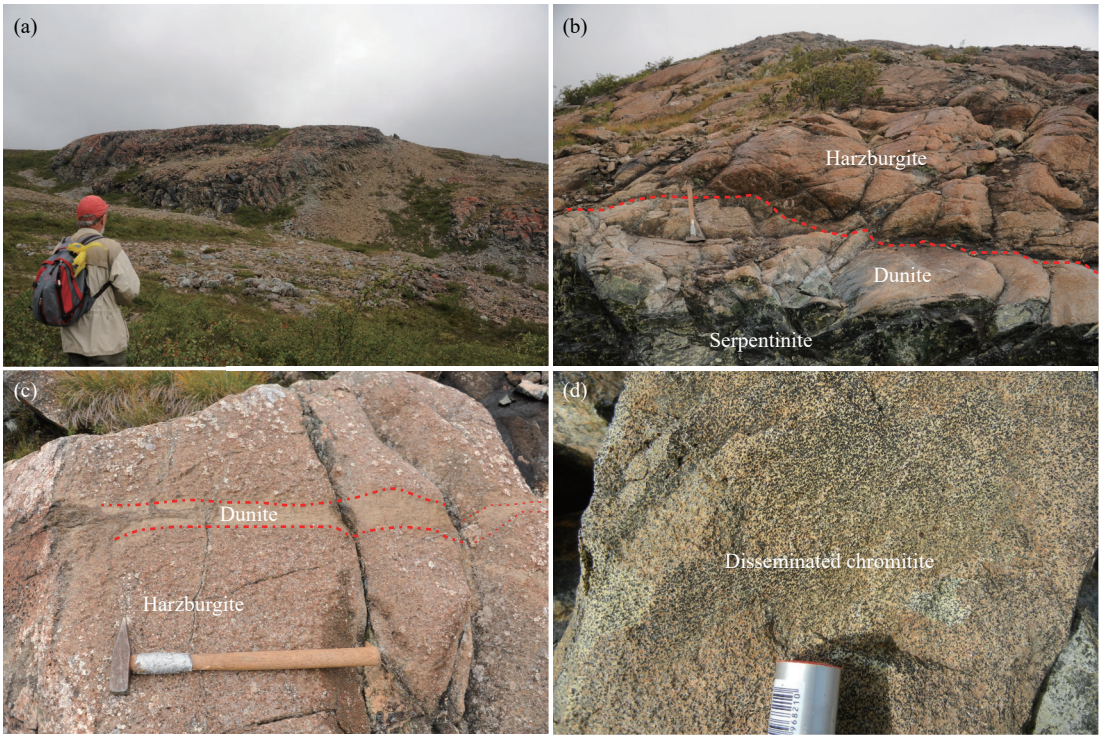

Fig. 2. Field photographs showing the various lithologies in the Feragen ophiolite. a–The Feragen ultramafic rocks; b and c–Dunite veins in harzburgite; d–Disseminated chromite ore.

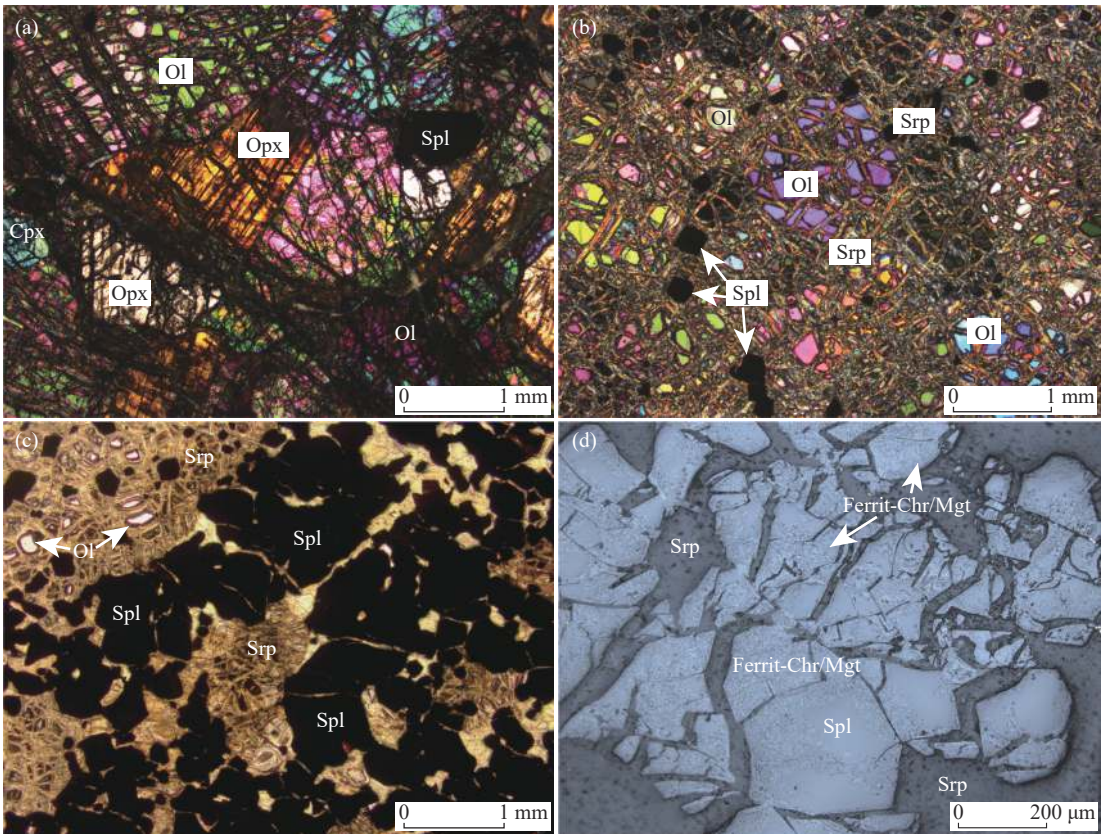

Fig. 3. Photomicrographs of peridotites and chromitites in the Feragen ophiolite. a–Harzburgite; coarse-grained olivine coexisting with orthopyroxene, granular texture (cross-polarized light); b–Dunite; olivine altered by serpentine along cracks and boundaries (cross-polarized light); c–Disseminated chromitites; olivine has been mostly altered by serpentine (plane-polarized light); d–Chromian spinels altered to ferrit-chromite or magnetite along boundaries and fractures in the disseminated chromitites (reflected light). Ol–olivine; Opx–orthopyroxene; Spl–chromian spinel; Cpx–clinopyroxene; Srp–serpentine; Ferrit-chr–Ferrit-chromite; Mgt–magnetite.

However, vermicular grains are also commonly observed in the chromitites. Chromian spinel grains are usually altered to ferrit-chromite or magnetite along boundaries and fractures, whereas olivines in the ores are mostly replaced by serpentine (Fig. 3d). Olivines are also observed as inclusions in the chromian spinel.

4. Sample preparation and analytical methods

Fresh harzburgite, dunite and chromitite samples were selected for petrographic examination and mineralogical analysis. The analyses were performed in the Key Laboratory of Nuclear Resources and Environment (East China Institute of Technology), Ministry of Education using a JEOL JXA-8100 electron microprobe with an Inca energy-dispersive spectrometer. The microprobe was set to operate at a voltage of 15 kV, a beam current of 20 amps and a spot diameter of 5 μm. Representative analyses of olivine, pyroxene and chromian spinel are presented in Tables 1–3, respectively.

Samples selected for whole-rock geochemical analysis were ground in an agate mill, after washing in distilled water and drying. Major elements were determined on fused glass beads by X-ray fluorescence (XRF) spectrometry. The analytical accuracy is estimated to be 1% relative for SiO_2 and 2% relative for the other oxides. Trace elements, including rare earth elements (REE), were determined by inductively coupled plasma-mass spectrometry (ICP-MS). GB/T14506.28-2010 standard (GSR3), GB/T14506.14-2010 standard (GSR5) and three internal standards were measured simultaneously to ensure consistency of the analytical results. Analytical uncertainties are estimated to be 10% for trace elements with abundances less than 10×10^{-6}, and around 5% for those higher than 10×10^{-6}. Platinum group elements (PGEs) of the peridotites and chromitites were analyzed using the nickel sulfide fire assay and Te-coprecipitation method of Jackson SE et al. (1990) and Sun SS et al. (1993) followed by ICP-MS measurements. Detailed procedures were described by Sun Y and Sun M (2005) and Dai JG et al. (2011). All of the analysis were determined in the National Research Center of Geoanalysis, Chinese Academy of Geological Sciences, Beijing. Representative analyses are shown in Tables 4 and 5.

5. Results

5.1. Mineral compositions

5.1.1. Olivines

All of the analyzed olivines are highly magnesian ($Fo_{89.8–90.7}$). Olivine in the harzburgite has Fo values of 89.8−90.2 with NiO contents of 0.33−0.39%, whereas olivine in the dunite has slightly higher Fo (89.9−90.7) with constant NiO contents (0.27−0.40%) (Fig. 4a). MnO contents of

Table 1. Representative microprobe analyses of olivine in the peridotites and chromitites of the Feragen ophiolite.

Lithology	Harzburgite							Dunite					chromitite							
Sample	S27-3-6	S27-3-7	S27-3-8	S27-3-9	S27-3-10	S27-3-11	S27-3-12	S27-2-6	S27-2-7	S27-2-8	S27-2-9	S27-2-10	S27-5-6	S27-5-7	S27-5-8	S27-4-6	S27-4-7	S27-4-8	S27-4-9	S27-4-10
SiO_2	40.86	40.65	40.39	40.77	40.52	40.69	40.73	41.33	40.32	40.92	40.83	40.82	42.50	41.43	42.92	43.01	42.56	42.97	43.34	42.32
Na_2O	0.00	0.01	0.00	0.00	0.00	0.01	0.02	0.02	0.01	0.01	0.02	0.00	0.01	0.01	0.01	0.02	0.02	0.01	0.01	0.00
Cr_2O_3	0.03	0.05	0.04	0.03	0.00	0.01	0.04	0.02	0.00	0.02	0.00	0.00	0.04	0.03	0.00	0.06	0.04	0.07	0.07	0.04
K_2O	0.00	0.00	0.00	0.02	0.02	0.00	0.00	0.00	0.00	0.02	0.01	0.00	0.01	0.01	0.02	0.00	0.00	0.00	0.01	0.00
MgO	48.59	48.58	48.61	49.03	48.36	49.12	48.53	48.52	49.31	49.46	49.07	49.92	53.36	52.00	52.27	53.05	53.84	53.19	52.63	53.09
Al_2O_3	0.01	0.00	0.00	0.00	0.00	0.00	0.01	0.00	0.02	0.00	0.00	0.01	0.01	0.18	0.00	0.12	0.02	0.00	0.07	0.09
MnO	0.12	0.11	0.16	0.12	0.13	0.10	0.13	0.09	0.15	0.09	0.14	0.10	0.02	0.07	0.09	0.05	0.14	0.09	0.11	0.08
CaO	0.14	0.01	0.03	0.01	0.02	0.04	0.02	0.00	0.02	0.02	0.00	0.01	0.05	0.01	0.09	0.04	0.06	0.02	0.07	0.03
FeO	9.58	9.46	9.39	9.69	9.66	9.58	9.88	9.72	9.15	9.01	9.22	9.36	2.21	4.74	3.01	2.57	2.70	2.82	2.64	2.15
TiO_2	0.00	0.00	0.00	0.03	0.03	0.00	0.00	0.00	0.00	0.00	0.00	0.00	0.01	0.00	0.00	0.00	0.02	0.05	0.06	0.00
NiO	0.35	0.36	0.39	0.35	0.39	0.39	0.33	0.27	0.40	0.34	0.33	0.34	0.46	0.56	0.68	0.55	0.65	0.35	0.54	0.58
Total	99.69	99.23	99.01	100.04	99.12	99.93	99.70	99.96	99.37	99.88	99.61	100.55	98.69	99.05	99.08	99.46	100.05	99.55	99.54	98.37
Fo	90.04	90.15	90.22	90.02	89.92	90.14	89.75	89.90	90.57	90.73	90.47	90.48	97.73	95.14	96.87	97.36	97.27	97.11	97.27	97.78

Table 2. Representative microprobe analyses of orthopyroxene and clinopyroxene in the harzburgites of the Feragen ophiolite.

Lithology	Orthopyroxene						Clinopyroxene					
Sample	S27-3-13	S27-3-14	S27-3-45	S27-3-46	S27-3-47	S27-3-48	S27-3-4	S27-3-5	S27-3-16	S27-3-17	S27-3-19	S27-3-20
SiO_2	55.69	54.98	53.58	55.12	54.69	54.52	51.57	53.12	52.53	53.48	53.18	52.23
Na_2O	0.03	0.00	0.00	0.00	0.00	0.00	0.12	0.12	0.17	0.11	0.14	0.18
Cr_2O_3	0.88	0.76	0.85	0.76	0.72	0.78	1.36	0.89	0.88	0.75	0.86	1.11
K_2O	0.02	0.00	0.02	0.00	0.02	0.00	0.00	0.00	0.00	0.00	0.01	0.00
MgO	32.23	32.18	33.45	32.18	32.23	33.22	16.33	16.41	16.53	16.63	16.99	16.08
Al_2O_3	3.54	3.50	3.54	3.50	3.54	3.50	3.84	2.60	2.79	2.38	3.05	3.60
MnO	0.13	0.11	0.13	0.11	0.13	0.11	0.13	0.07	0.06	0.06	0.09	0.10
CaO	1.40	1.34	1.40	1.34	1.40	1.34	24.33	25.00	25.04	23.64	22.56	24.67
FeO	6.23	6.08	5.60	6.08	6.13	6.08	2.37	2.07	2.12	1.95	2.31	2.17
TiO_2	0.03	0.00	0.01	0.00	0.00	0.02	0.02	0.00	0.01	0.07	0.00	0.08
NiO	0.07	0.09	0.07	0.09	0.07	0.09	0.02	0.05	0.03	0.03	0.00	0.04
Total	100.25	99.05	98.65	99.18	98.94	99.66	100.10	100.32	100.14	99.10	99.19	100.27
En	87.75	88.03	88.97	88.03	87.88	88.36	46.46	46.17	46.28	47.91	49.25	45.90
Fs	9.51	9.33	8.35	9.33	9.37	9.07	3.78	3.26	3.33	3.15	3.75	3.48
Wo	2.74	2.63	2.68	2.63	2.75	2.56	49.76	50.56	50.39	48.94	47.00	50.62
Mg#	90.22	90.42	91.42	90.42	90.37	90.69	92.47	93.40	93.30	93.84	92.93	92.95

Table 3. Representative microprobe analyses of chromian spinel in the peridotites and chromitites.

Lithology	harzburgite				Dunite								Chromitite					
Sample	S27-1-1	S27-1-2	S27-1-3	S27-3-18	S27-2-1	S27-2-2	S27-2-3	S27-2-4	S27-2-5	S27-3-1	S27-3-2	S27-3-3	S27-3-4	S27-3-5	S27-4-1	S27-4-2	S27-4-3	S27-4-4	S27-4-5	S27-4-6
SiO_2	0.04	0.06	0.04	0.06	0.06	0.03	0.02	0.06	0.01	0.07	0.02	0.03	0.05	0.03	0.06	0.00	0.01	0.13	0.18	0.10
Na_2O	0.04	0.03	0.04	0.03	0.02	0.02	0.0	0.02	0.00	0.03	0.00	0.01	0.00	0.03	0.05	0.02	0.03	0.06	0.00	0.03
Cr_2O_3	27.86	25.68	28.00	25.57	54.64	54.82	54.98	53.97	53.92	53.41	54.10	53.82	54.42	53.92	51.46	53.99	51.21	50.92	49.36	50.78
K_2O	0.01	0.00	0.01	0.00	0.00	0.00	0.00	0.00	0.02	0.00	0.00	0.01	0.00	0.01	0.01	0.00	0.00	0.00	0.00	0.00
MgO	17.03	16.85	17.20	17.00	16.07	16.02	15.89	14.57	13.71	11.95	14.16	14.31	14.02	13.33	6.38	7.98	6.82	7.14	12.51	7.56
Al_2O_3	40.11	41.99	40.11	41.99	14.47	14.38	14.51	14.01	13.75	13.34	13.70	13.63	13.61	13.77	6.13	8.18	9.48	6.67	10.98	6.46
MnO	0.20	0.21	0.20	0.21	0.26	0.27	0.25	0.30	0.35	0.35	0.24	0.29	0.30	0.29	0.71	0.96	0.97	1.00	0.81	0.92
FeO	14.43	14.11	14.49	14.18	14.30	14.09	14.14	16.99	17.88	19.97	17.07	17.16	17.10	18.44	34.27	28.49	30.88	32.94	25.69	32.24
TiO_2	0.03	0.00	0.03	0.00	0.19	0.12	0.22	0.21	0.16	0.25	0.20	0.20	0.16	0.16	0.08	0.22	0.22	0.18	0.16	0.20
NiO	0.16	0.14	0.16	0.14	0.13	0.16	0.04	0.05	0.10	0.10	0.07	0.07	0.07	0.05	0.11	0.14	0.09	0.04	0.13	0.16
Total	99.89	99.06	100.27	99.18	100.11	99.90	100.05	100.17	99.90	99.47	99.54	99.52	99.72	100.03	99.25	99.98	99.72	99.07	99.83	98.45
Mg#	68.29	68.59	68.40	68.65	67.45	67.39	67.13	61.20	58.05	52.40	60.01	60.27	59.88	56.79	25.18	33.49	28.45	28.44	47.46	29.95
Cr#	31.78	29.09	31.89	29.00	71.70	71.89	71.77	72.10	72.45	72.87	72.60	72.60	72.84	72.43	84.91	81.58	78.37	83.67	75.10	84.06
Fe^{3+}#	0.40	0.41	0.40	0.41	0.66	0.38	0.38	0.73	0.31	0.90	0.36	0.49	0.51	0.51	0.82	0.39	0.50	1.57	1.60	1.26

Mg#=100Mg/Mg+Fe^{2+}, Fe^{3+}#=100Fe^{3+}/Cr+Al+Fe^{3+}

olivine in the harzburgite are 0.10−0.16%, which are essentially the same with that in the dunite (MnO content ranging from 0.09−0.15%) (Fig. 4b). Olivines in the chromitites have Fo values ranging from 95.1−97.8, which are much higher than olivines in the harzburgite and dunite.

5.1.2. Pyroxenes

Only orthopyroxene and clinopyroxene in the harzburgite are analyzed as those in the dunite and chromitite have been completely altered. The enstatite (En) contents of orthopyroxene in harzburgite range from 87.7 to 89.0 (Table 2). The Al_2O_3 and Cr_2O_3 contents are 3.50%−3.54% and 0.72%−0.88%, respectively (Figs. 5a–b). The Mg# values of orthopyroxene range from 90.2−91.4.

Clinopyroxene in harzburgite is diopside with En values of 45.9−49.3 (Table 2). It has Mg# values varying from 92.5 to 93.8. The Al_2O_3 contents of clinopyroxene vary from 2.38%−3.84%, which show a negative correlation with the Mg# values (Fig. 5c). The Cr_2O_3 contents are variable ranging from 0.75% to 1.36%, showing positive correlations with Al_2O_3 of clinopyroxene (Fig. 5d).

5.1.3. Chromian spinels

Chromian spinels in the harzburgite have low Cr# values of 29.0−31.9 and high Mg# values of 68.3−68.7, whereas those in the dunites have much higher Cr#s (71.7−72.9) but lower Mg#s (52.4−67.5) (Table 3). TiO_2 contents of chromian spinels in the harzburgites are $<$ 0.03%, and those in the dunite samples are up to 0.25%. The chromitites in the Feragen ophiolite belong to the high-Cr type with Cr# values ranging from 75.1−84.9 and Mg# values ranging from 25.2−47.5. TiO_2 contents of chromian spinels in the chromitite are from 0.08% to 0.22%.

5.2. Whole-rock geochemistry

5.2.1. Major geochemistry

All the samples are Mg-rich (MgO contents ranging from 41.35%−44.99%), Al-poor (0.20−1.13% Al_2O_3) and alkali-poor (<0.1% Na_2O)(Table 4). The harzburgites have MgO contents ranging from 41.35%−41.82%, which are lower than those of dunites (43.62%−44.99% MgO). However, the contents of CaO (1.06−1.37%), Al_2O_3 (1.07%−1.13%) and TiO_2 (0.02%−0.05%) of the harzburgites are much higher than those of dunites (0.18%−0.82% CaO, 0.20%−0.60% Al_2O_3 and <0.01% TiO_2). It shows a relatively linear decrease in CaO, Al_2O_3, and TiO_2 with increasing MgO content, respectively, from harzburgite to dunite (Figs. 6a–c). Total iron as FeO* in the harzburgites are also higher than those in the dunites, representing a negative correlation with MgO contents (Fig. 6d). The Feragen harzburgites are comparable with SSZ-type peridotite, whereas the dunites are comparable with abyssal (or MOR-type) varieties as shown by whole-rock geochemistry (Figs. 6 and 7).

5.2.2. Trace element geochemistry

The analyzed harzburgite and dunite samples have ∑REE

Table 4. Major and trace element compositions of whole-rock samples of peridotite in the Feragen ophiolite.

Lithology	Harzburgite			Dunite			
Sample	YLS13-27-4	YLS13-27-6	YLS13-27-7	YLS13-27-8	YLS13-27-1	YLS13-27-2	YLS13-27-3
Major oxides/wt%							
SiO_2	39.91	40.69	40.39	34.72	36.52	34.88	38.68
Al_2O_3	1.07	1.13	1.08	0.52	0.48	0.20	0.60
CaO	1.06	1.37	1.16	0.22	0.22	0.18	0.82
Fe_2O_3	2.94	2.87	3.24	1.94	3.55	2.11	2.80
FeO	4.97	4.90	4.49	2.23	3.35	3.40	3.54
K_2O	b.d.	b.d.	b.d.	b.d.	b.d.	b.d.	b.d.
MgO	41.82	41.35	41.59	44.99	44.00	44.56	43.62
MnO	0.12	0.12	0.12	0.09	0.10	0.09	0.08
Na_2O	b.d.	b.d.	b.d.	b.d.	b.d.	b.d.	b.d.
P_2O_5	b.d.	b.d.	b.d.	b.d.	b.d.	b.d.	b.d.
TiO_2	0.05	0.02	b.d.	0.01	b.d.	0.01	b.d.
H_2O^+	8.18	8.22	8.76	15.16	12.32	15.24	10.22
LOI	8.36	8.44	8.77	15.27	12.56	15.40	10.66
Trace elements/$\times10^{-6}$							
Ta	0.041	0.032	0.029	0.036	0.030	0.034	0.036
Th	0.021	0.019	0.011	0.010	0.038	0.015	0.023
U	0.010	0.010	0.007	0.007	0.009	0.005	0.011
Pb	0.12	0.18	0.16	0.12	2.93	0.21	0.24
Ga	1.05	1.08	1.08	0.97	0.81	0.21	0.79
Sr	0.46	0.40	0.35	0.39	1.41	0.98	1.01
V	42.4	46.3	42.2	15.0	13.3	5.16	30.5
Rb	0.77	0.77	0.72	0.31	0.45	0.19	0.53
Nb	0.26	0.22	0.21	0.24	0.22	0.23	0.21
Ba	1.37	0.86	0.65	0.33	2.35	1.37	1.07
Zr	0.23	0.36	0.18	0.15	0.53	0.22	0.27
Hf	0.008	0.011	0.005	0.004	0.014	0.005	0.009
Cr	1993	2139	1985	2284	1871	914	2435
Ni	1600	1521	1563	1909	1717	2077	1648
Co	120	116	117	116	118	112	118
Cu	7.18	9.21	14.7	8.85	5.47	5.69	5.97
Zn	41.9	42.6	45.7	25.4	22.7	25.9	32.3
Cs	0.19	0.20	0.16	0.16	0.29	0.07	0.25
Sc	10.4	11.1	10.2	4.63	5.33	3.05	7.89
La	0.041	0.022	0.020	0.021	0.093	0.030	0.048
Ce	0.069	0.039	0.030	0.039	0.170	0.058	0.075
Pr	0.010	0.006	0.005	0.004	0.020	0.008	0.009
Nd	0.040	0.025	0.019	0.017	0.050	0.017	0.033
Sm	0.017	0.009	0.003	0.005	0.012	0.001	0.011
Eu	0.003	0.003	0.002	0.000	0.004	0.002	0.003
Gd	0.032	0.019	0.016	0.005	0.025	0.011	0.017
Tb	0.004	0.005	0.003	0.001	0.002	0.001	0.004
Dy	0.031	0.032	0.040	0.014	0.012	0.010	0.021
Ho	0.007	0.014	0.009	0.003	0.002	0.001	0.006
Er	0.044	0.046	0.042	0.014	0.011	0.007	0.019
Tm	0.006	0.006	0.007	0.003	0.001	0.001	0.003
Yb	0.066	0.063	0.051	0.016	0.017	0.007	0.028
Lu	0.011	0.010	0.012	0.004	0.003	0.003	0.005
Y	0.28	0.31	0.28	0.090	0.080	0.040	0.16

of 0.26×10^{-6}–0.38×10^{-6} and 0.15×10^{-6}–0.42×10^{-6}, respectively (Table 4), both of which are well below primitive mantle values indicating significant depletion presumably by high degrees of partial melting (Miller C et al., 2003). In the chondrite-normalized REE diagram, all harzburgites have weakly spoon-shaped patterns with relative enrichment in both LREE and HREE and depletion in MREE (Fig. 8a), which is consistent with the patterns displayed by abyssal peridotites with low REE contents and enrichment of HREE (Niu Y, 2004). The dunites are characterized by lower HREE

Table 5. Platinum-group element compositions of whole-rock samples of peridotite and chromitite in the Feragen ophiolite (10^{-9}).

Lithology	Harzburgite			Dunite				Chromitite
Sample	YLS13-27-4	YLS13-27-6	YLS13-27-7	YLS13-27-8	YLS13-27-1	YLS13-27-2	YLS13-27-3	YLS13-27-5
Os	3.51	5.69	4.32	2.97	3.16	4.51	3.29	19.6
Ir	1.50	2.52	1.45	1.58	1.48	2.38	1.74	8.54
Ru	4.94	6.64	4.99	3.97	3.98	3.30	4.29	37.5
Rh	0.94	1.24	1.22	0.65	0.78	0.39	0.71	3.17
Pt	5.09	6.48	6.86	2.27	3.25	0.94	3.65	0.62
Pd	4.09	5.93	5.92	1.94	0.27	0.20	1.44	0.12
Total PGE	20.1	28.5	24.8	13.4	12.9	11.7	15.1	69.6
Pd/Ir	2.73	2.35	4.08	1.23	0.18	0.08	0.83	0.01
Pt/Pd	1.24	1.09	1.16	1.17	12.04	4.70	2.53	5.17

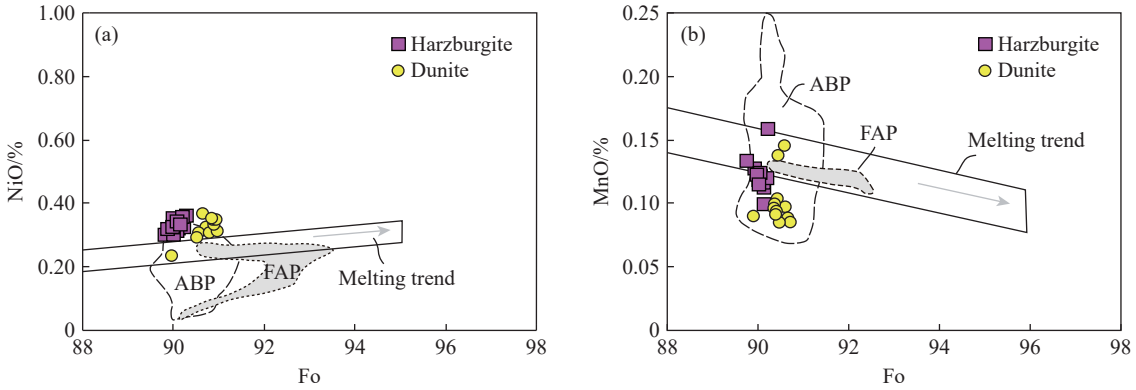

Fig. 4. NiO (a) and MnO (b) *vs.* Fo contents of olivine in the different lithologies of the Feragen ophiolite. ABP–abyssal peridotite and FAP–fore-arc peridotite from Pagé P et al. (2008), partial melting trends from Ozawa K (1994), and fractionation trends from Ozawa K (1994) and Nakamura M (1995).

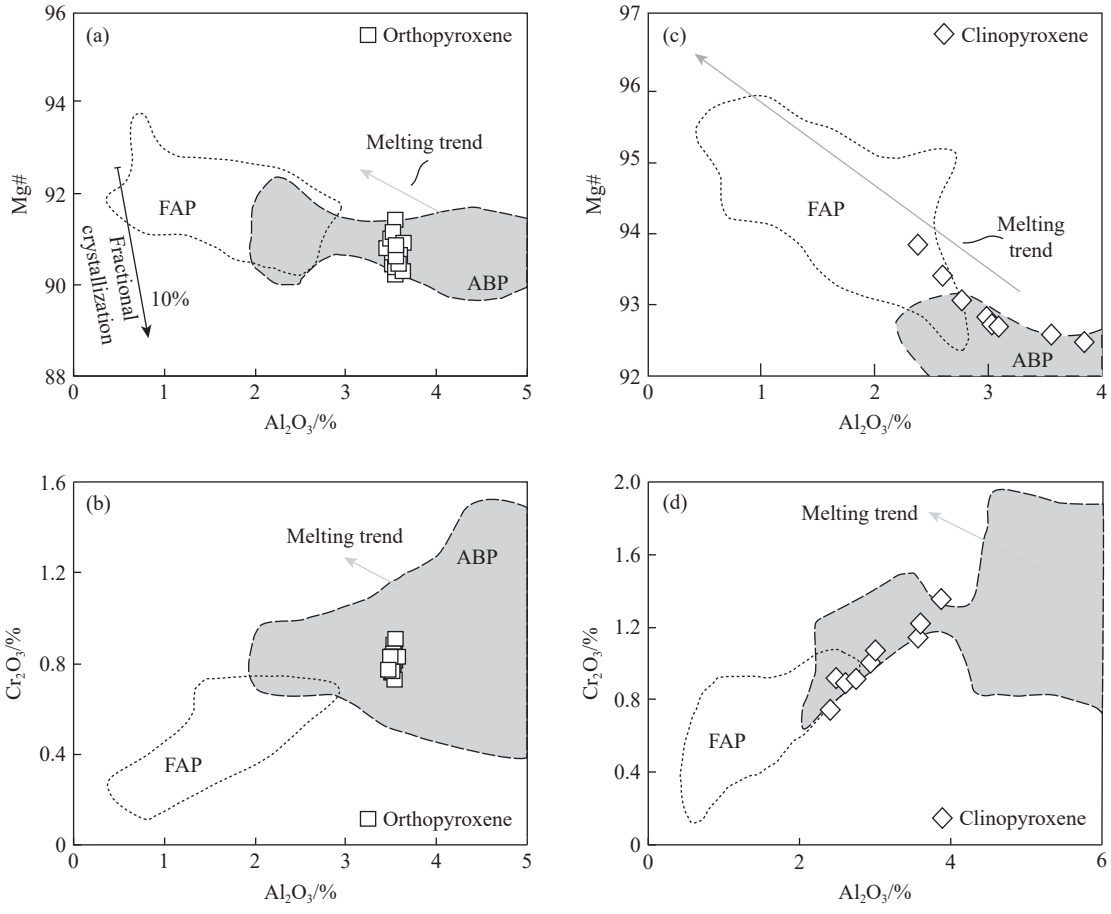

Fig. 5. Compositional range of orthopyroxene (a–b) and clinopyroxene (c–d) in harzburgites of the Feragen ophiolite. ABP-abyssal peridotite and FAP-fore-arc peridotite from Pagé P et al. (2008). The melting trend from Smith SE and Elthon D (1988).

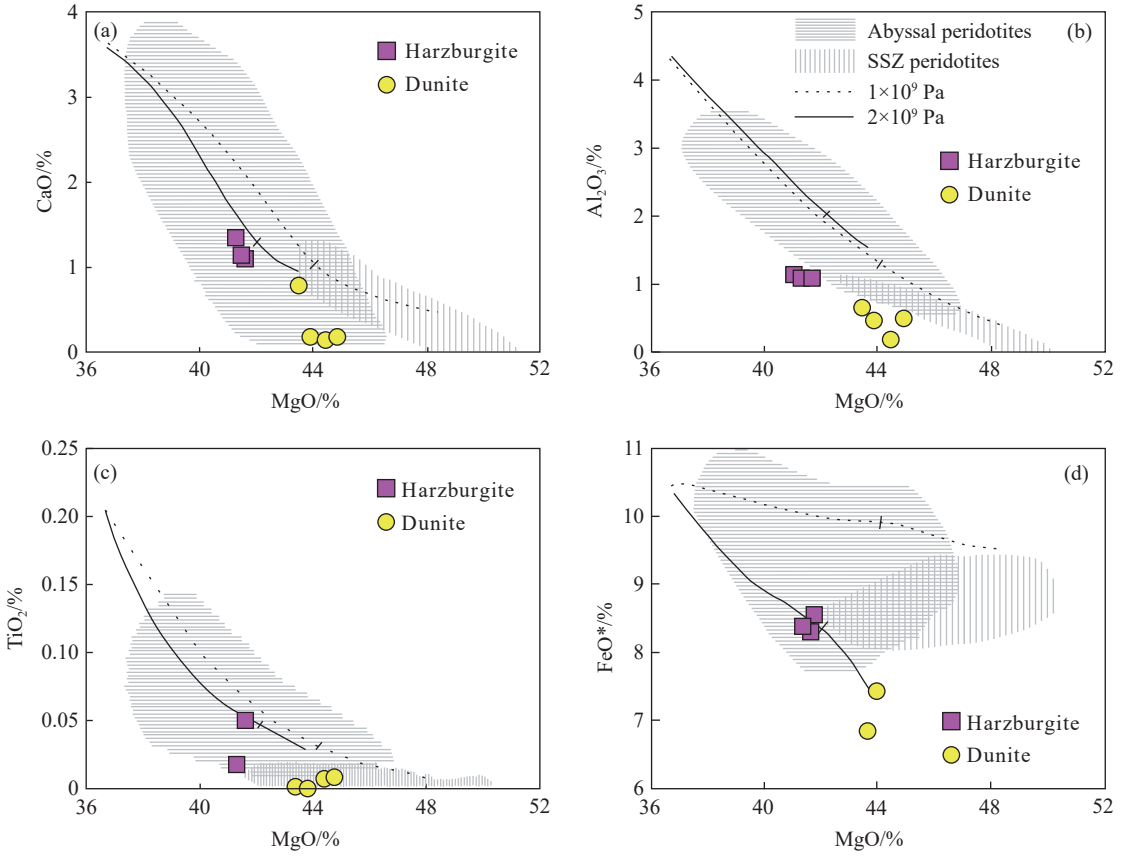

Fig. 6. Harker diagrams of the whole-rock compositional range of harzburgites and dunites in the Feragen ophiolite. Abyssal and SSZ peridotite fields from Niu Y et al. (1997), Parkinson IJ and Pearce JA (1998) and Uysal I et al. (2009). The residual compositions from melting (at 1×10^9 Pa and 2×10^9 Pa) of Primitive Mantle (Palme H and O'Neill HSC, 2004) calculated using pMELTS program of maximum 40% melting degree (Ghiorso MS et al., 2002) are also shown in the diagram.

concentrations than harzburgites, representing stronger depletion and resembling forearc peridotites (Parkinson IJ and Pearce JA, 1998) (Fig. 8a).

All of the harzburgites and dunites also have similar primitive mantle-normalized trace element patterns with concentrations well below those of primitive mantle (Fig. 8b). They display strongly depletion in REE and weakly depletion in highly incompatible elements (Rb, Ba, Th, U, V, Sc, Nb and Ta). The dunites are characterized by stronger depletion in V, Sc, Y and HREE than the harzburgites (Fig. 8b), which also show negative correlations with the MgO contents in dunites and harzburgites (Fig. 7).

5.2.3. Platinum group element (PGE)

The analyzed harzburgite and dunite samples have total PGE concentrations of 20.1×10^{-9}–28.5×10^{-9} and 11.7×10^{-9}–15.1×10^{-9}, respectively, both of which are lower than those of analyzed chromitites ($\sum$PGE = 69.6×10^{-9}) (Table 5). The chromitites are significantly enriched in the Iridium-group PGE (IPGE: Os, Ir and Ru; 65.6×10^{-9}) relative to the Palladium-group PGE (PPGE: Rh, Pt and Pd; 3.9×10^{-9}).

The analyzed harzburgites display similar patterns with primitive mantle in the primitive mantle-normalized PGE patterns (Fig. 9a). However, the dunites are characterized by a common depletion in Pt and Pd (Figs. 9a–b). The chromitites show generally greater Os, Ir, Ru, and Rh concentrations than harzburgites and dunites, but are extremely depleted in both Pt and Pd. The analyzed chromitites have lowest Pd and Pd/Ir ratios than harzburgites, dunites and also the primitive mantle (Fig. 9c).

6. Discussion

6.1. Oxygen fugacity of the Feragen peridotites and chromitites

Peridotites in mantle wedges of the supra-subduction zone are generally more oxidized than upper mantle peridotites in other tectonic settings (Parkinson IJ and Arculus RJ, 1999). Dehydration of subducted oceanic lithosphere plays an important role on the formation of subduction-related melts and the transformation of ferrous iron to ferric iron in melts (Acrulus RJ, 1994).

The Oxygen fugacity (fO_2) values of parental magmas of peridotites and podiform chromitites can be calculated based on the thermometers of coexisting olivine, orthopyroxene, and chromian spinel (O'Neill H and Wall V, 1987; Ballhaus C et al., 1991; Sack RO and Ghiorso MS, 1991; Qiao GB et al., 2023). Due to the rarity of orthopyroxene in the Feragen chromitites and dunites, coexisting olivine-chromian spinel pairs in harzburgites, dunites and chromitites were used to estimate fO_2 values of their sourced magma. Using the

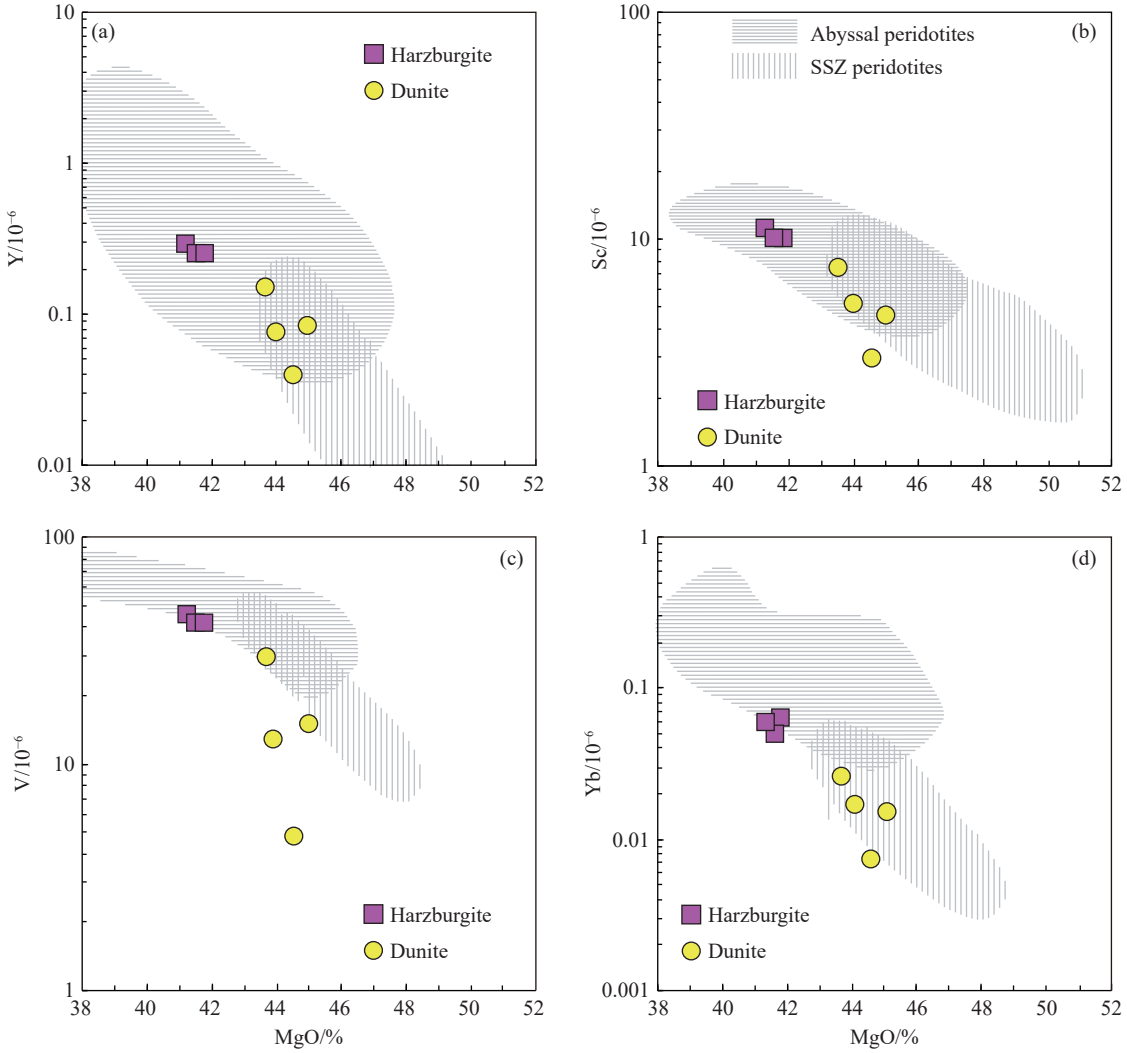

Fig. 7. Variation diagrams of MgO vs. Y (a), Sc (b), V (c), and Yb (d) in harzburgite and dunite samples of the Feragen ophiolite. Abyssal and SSZ peridotite fields from Niu Y et al. (1997) and Parkinson IJ and Pearce JA (1998), respectively.

method of Wan Z et al. (2008), ▲logfO2—reported as log units relative to the fayalite-magnetite-quartz (FMQ) buffer at 1 GPa —is calculated from olivine-spinel equilibrium geothermal data (Ballhaus C et al., 1991)(Table 6).The fO_2 are reported as log units relative to the fayalite-magnetite-quartz (FMQ) buffer at 1.0GPa (Table 6). The more oxidized values of −0.17–+0.23 and +2.78–+5.65 are reported for dunites and chromitites, respectively, whereas fO_2 values of harzburgites (−2.19–−1.58) are below the FMQ buffer (Fig. 10a). The highly oxidized dunites and chromitites are consistent with the formation as mantle wedge above a subduction zone (Pearce JA et al., 2000). The pronounced increase in both fO_2 and Cr# values of chromian spinel from harzburgites to dunites and chromitites might be a result of melt-rock interaction. The interaction between harzburgites, which have back-arc basin geochemical features, with highly oxidized, supra-subduction zone melts, produced the analyzed dunites and chromitites.

6.2. Evolution of the Feragen peridotites and chromitites

As produced by crystallization from parental magmas, the compositions of chromian spinel are generally used by many researchers as a sensitive petrogenetic indicator to constrain the parental melt evolution (Dick HJ and Bullen T, 1984; Arai S, 1994; Zhou MF et al., 1996; Barnes SJ and Roeder PL, 2001; Kamenetsky VS et al., 2001; Rollinson H, 2008). Experimental studies have shown that Al_2O_3 and FeO/MgO contents in chromian spinels are directly related to the compositions of parental melt (Maurel C and Maurel P, 1982; Kamenetsky VS et al., 2001). The Al_2O_3 and FeO/MgO contents of parental melt can be calculated as a function of Al_2O_3 and FeO/MgO in chromian spinels using the equation introduced by Maurel C and Maurel P (1982) and Augé T (1987), respectively. Results are presented in Table 6. The calculated Al_2O_3 contents and FeO/MgO ratios of the parental melts for the Feragen dunites are 11.80−12.07% and 0.74−1.09, respectively, both of which scatter in the field of boninitic rocks (Wilson M, 1989; Fig. 10b). Compared with primitive magmas that are ascribed for different tectonic settings, the Al_2O_3 contents of the parental melts for the Feragen chromitites (8.41−11.45%) also scatter in the field of boninite (Fig.10b). However, the parental melts have much

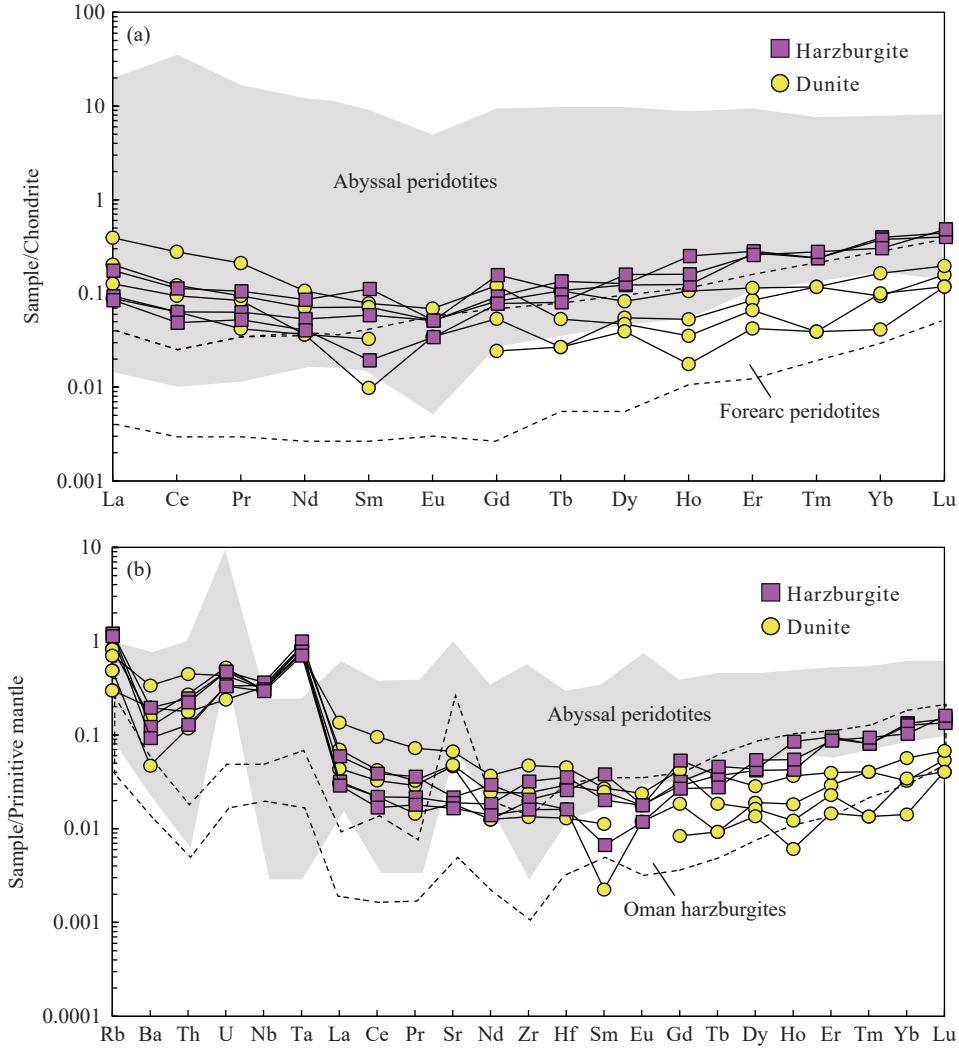

Fig. 8. a–Chondrite-normalized REE patterns of dunites and harzburgites in the Feragen ophiolite (normalized after McDonough WF and Sun SS, 1995). b–Primitive mantle-normalized trace element spider diagrams of dunites and harzburgites in the Feragen mantle ophiolite (normalized after McDonough WF and Sun SS, 1995). Fields of abyssal peridotites (afterBodinier JL and Godard M, 2003; Niu Y, 2004) and forearc peridotites (Parkinson IJ and Pearce JA, 1998) are shown for comparison. The compositions of harzburgites sampled in the Semail (Oman) ophiolite from Godard M et al. (2000).

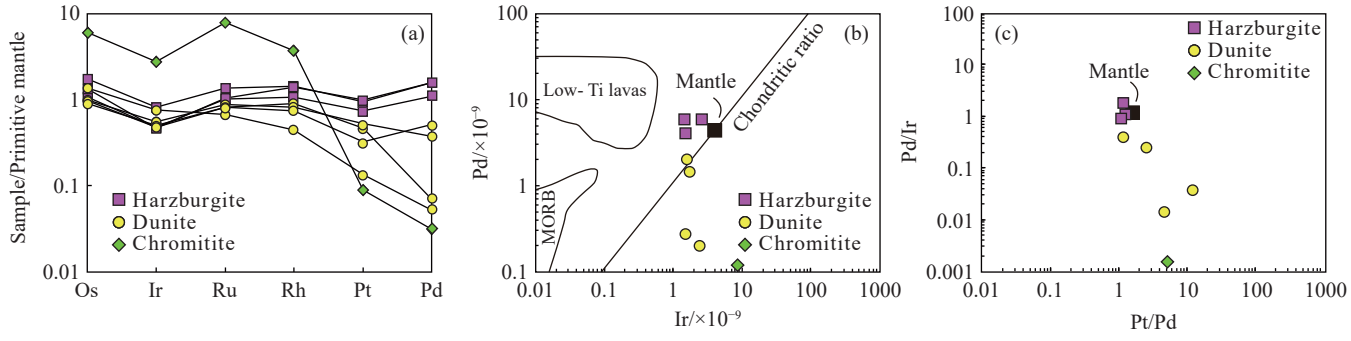

Fig. 9. a–Primitive mantle-normalized PGE patterns of the Feragen peridotite and chromitites (normalized after Barnes SJ et al. (1988); b–Iridium *vs.* palladium of the peridotites and chromitites in the Feragen ophiolite. Chondritic ratio and mantle values from Chou CL et al. (1983). MORB and low-Ti lava fields from Hamlyn PR et al. (1985); c–Platinum/iridium *vs.* palladium/platinum for peridotites and chromitites in the Feragen ophiolite. Primitive mantle values from Barnes SJ et al. (1988).

higher FeO/MgO ratios (1.65−3.92) than dunites and boninitic rocks. As similar with the highly oxidized values of chromitites (Fig. 10a), this study suggest that the high FeO/MgO ratios for chromitites might have resulted from subsolidus re-equilibration and the ferrit-chromite alteration of chromian spinels (Fig. 3d).

It is known that Al contents of pyroxene and spinel are sensitive to the partial melting of mantle rocks and that they

Table 6. fO_2 and calculated melt in the Feragen peridotites and chromitites.

Lithology	Sample	Al_2O_3	FeO/MgO	Al_2O_3(melt)	YAl/spinel	YFe^{3+}/spinel	(FeO/MgO)melt	$\Delta\log fO_2$ (FMQ)	Cr#
Harzburgite	S27-1-1	40.11			0.68	0.004		−1.58	31.78
	S27-1-2	41.99			0.71	0.004		−2.13	29.09
	S27-1-3	40.11			0.68	0.004		−1.65	31.89
	S27-1-4	41.99			0.71	0.004		−2.19	29.00
Dunite	S27-2-6	14.47	0.89	12.05	0.28	0.007	0.75	−0.03	71.70
	S27-2-7	14.38	0.88	12.02	0.28	0.004	0.74	0.01	71.89
	S27-2-8	14.51	0.89	12.07	0.28	0.004	0.75	−0.17	71.77
	S27-2-9	14.01	1.17	11.89	0.28	0.007	0.98	0.23	72.10
	S27-2-10	13.75	1.30	11.80	0.27	0.003	1.09	0.18	72.45
Chromitite	S27-4-1	8.73	10.33	8.41	0.24	0.009	3.92	5.65	84.91
	S27-4-2	1.18	7.23	9.92	0.04	0.010	2.71	2.78	81.58
	S27-4-3	1.29	16.32	10.69	0.05	0.014	3.34	4.04	78.37
	S27-4-4	2.76	7.36	8.85	0.09	0.013	3.39	5.00	83.67
	S27-4-5	8.15	9.04	11.45	0.21	0.004	1.65	4.24	75.10
	S27-4-6	6.98	7.75	8.69	0.19	0.005	3.13	4.63	84.06

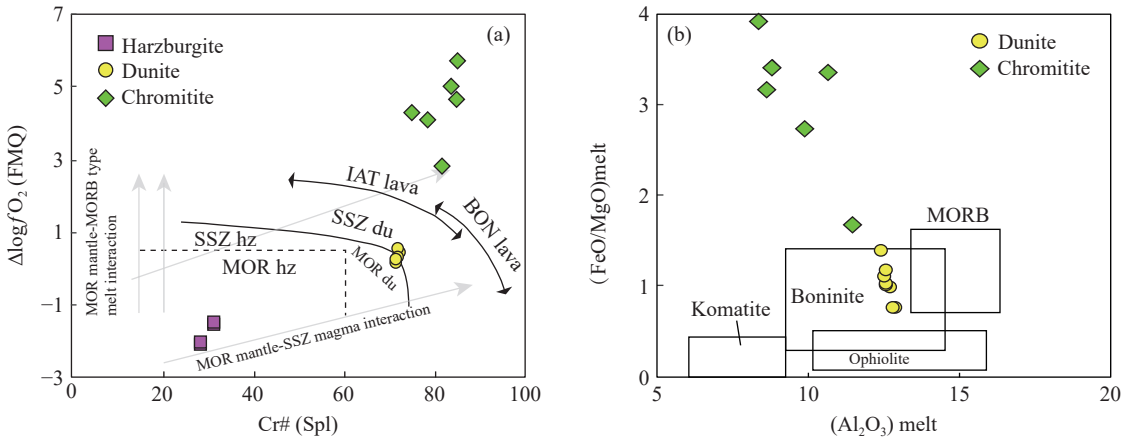

Fig. 10. a–Plot of $\Delta\log fO_2$ (FMQ) *vs.* Cr# of spinels from the Feragen chromitite, harzburgites and dunites. We have calculated $\Delta\log fO_2$ (Ballhaus C et al., 1991) from geothermometric data derived from olivine - spinel equilibria following the approach of Wan Z et al. (2008); the data are provided in Table 6. MOR–SSZ discrimination boundaries for dunites (solid line) and harzburgites (dashed line) are shown. MOR–mid-ocean ridge, SSZ–supra-subduction zone, BAB–back arc basin, BON–boninite, IAT–island arc tholeiite (Parkinson IJ and Pearce JA, 1998; Dare SAS et al., 2009); b–(FeO/MgO) melt vs (Al_2O_3) melt (%) calculated on the basis of the chemical composition of the Feragen dunites and chromitites. Tectonic discrimination fields from Barnes SJ and Roeder PL (2001).

decrease systematically as the peridotites become more depleted (Dick HJ and Natland JH, 1996; Zhou MF et al., 2005). Due to the common alteration observed in the Feragan ophiolite (Moore AC and Hultin I, 1980; Dunkel KG et al., 2019), fresh pyroxene grains are only analyzed in the Feragen harzburgites. The clinopyroxene and orthopyroxene in the Feragen harzburgites plot in the fields of abyssal peridotites (Fig. 5; Pagé P et al., 2008). The chromian spinels in the Feragen harzburgites plot within the MORB field of the Cr# versus Mg# discrimination diagram, and appear to be depleted about 15−20% with respect to the primitive upper mantle by low-degree partial melting (Figs. 11a–b). However, the chromian spinels in dunites plot within the forearc field in the Cr# versus Mg# discrimination diagram, and are more depleted >40% (Figs. 11a–b). Dunites occur as lenses in harzburgites of the Feragen ophiolite with high content of TiO_2 in chromian spinels (Figs. 2b–c; Table 3), suggesting a melt-rock origin. This interpretation is also supported by the depletion of PPGE concentrations in dunites with respect to harzburgites (Fig. 9), as PPGEs are more easily accessed during the melt-rock interaction.

Harzburgites and dunites in the Feragen ophiolite have well-developed, spoon-shaped REE patterns, which indicating weak LREE enrichment and reflecting the low-temperature secondary processes such as serpentinization, oceanic alteration or contamination by subduction-derived fluids (Miller C et al., 2003). It also consistent with the patterns for MORB-type mantle that has been refertilized in a SSZ setting. As the Feragen ophiolite was formed in a back-arc environment prior to tectonic emplacement during the orogenesis which produced the Trondheim Nappe (Moore AC and Hultin I, 1980), this study suggest that the Feragen harzburgite represent residues of low-degree partial melting in a back-arc setting, and then were modified by boninitic melts and fluids in a SSZ setting during intra-oceanic subduction, thus, producing the high-Cr chromitites.

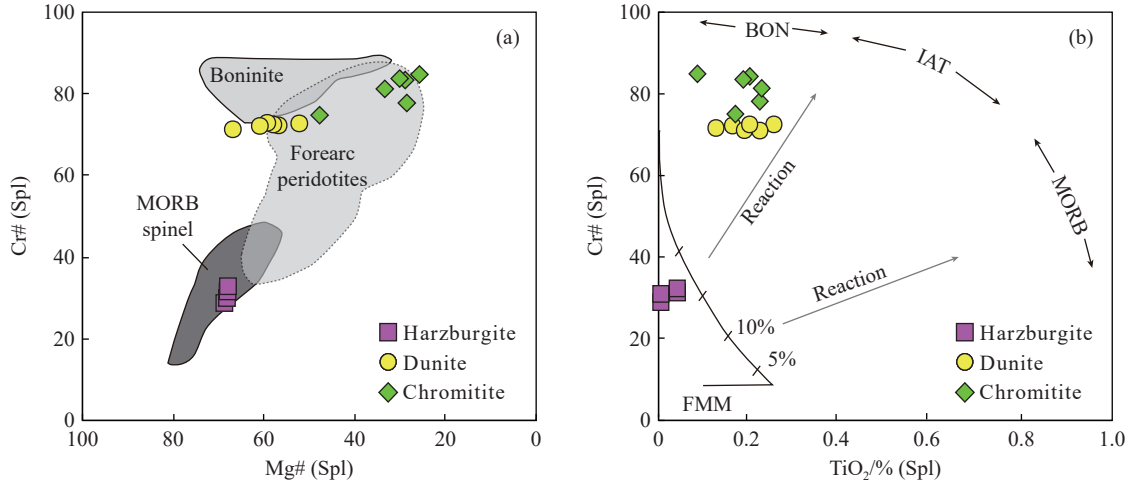

Fig. 11. a–Compositional range of chromian spinel in different lithologies of the Feragen ophiolite after Pearce JA et al. (2000). Data of spinels of MORB, forearc peridotites and boninites are form Izu-Bonin-Mariana system (Pearce JA et al., 2000, and references there in); b–Compositional relationship between Cr# and TiO_2 content of spinel in peridotite and chromitite samples.

6.3. Prospecting potential of chromitites

The Feragen ophiolite has been mined extensively for chromite and was the most important source of chrome in Norway until mining ceased around 1927. Several hundred small open pits and about 20 shafts were operated for open-pit and underground mining, respectively. Ore horizons are variable in size and have been recorded as bands up to 280 m long, 60−80 m deep, and with a maximum width of 1.5 m (Moore AC and Hultin I, 1980). It is believed to contain enough unmined chromite at practical minable depths to equal or exceed that mined to date, but the individual deposits are likely to be small. The fact that dunites and chromitites in the Feragen ophiolite are the product of melt-rock interaction and chromite ores are commonly associated with dunite veins scattering through the harzburgites, which provides dunite vein as a favorable prospecting criterion to chromite exploration in this area. Several large ultramafic bodies occur along the southern and eastern margins of the Trondheim Nappe Complex (Moore AC and Hultin I, 1980; Nilsson LP et al., 1997, 2005), all of which experienced the same tectonic evolution and ore mineralization as the Feragen ophiolite, thus having potential for further prospecting.

7. Conclusion

The Feragen peridotites display textural and geochemical evidence for multi-stage of partial melting, depletion, and refertilization at various scales. The less depleted harzburgites represent residues of low-degree partial melting in a back-arc setting. The formation of high-Cr chromitites and dunites together with the mineral and whole-rock geochemical features clearly refer to a supra-subduction setting. The calculated oxygen fugacity values for the Feragen dunites and chromitites are generally above the FMQ buffer, consistent with oceanic-arc mantle wedge above a subduction zone. The variable oxygen fugacity values in the same ophiolite can be explained by the interaction between boninitic melts or fluids with refractory harzburgite processing a back-arc setting. All of the available evidences suggest that the Feragen ophiolite has a complex tectonic history passing through back-arc to supa-subduction zone environment prior to being emplaced on land.

CRediT authorship contribution statement

Tian Qiu and Fa-hui Xiong developed the theoretical formalism and performed the analytic calculations. Tian Qiu wrote the manuscript with support from Fa-hui Xiong. All authors discussed the results and contributed to the final manuscript.

Declaration of competing interest

The authors declare no conflicts of interest.

Acknowledgments

This research was financially supported by the National Natural Science Foundation of China (92062215, 41720104009, 42172069), the China Geological Survey (DD20221886, DD20221817, DD20221657, DD20230340, DD20221630), the Key Special Project for Introduced Talents Team of Southern Marine Science and Engineering Guangdong Laboratory (Guangzhou) (GML2019ZD0201) and the Second Tibetan Plateau Scientific Expedition and Research Program (2019QZKK0801).

References

Ahmed A, Arai S. 2002. Unexpectedly high-PGE chromitite from the deeper mantle section of the northern Oman ophiolite and its tectonic implications. Contributions to Mineralogy and Petrology, 143, 263–278. doi: 10.1007/s00410-002-0347-8.

Arai S, Yurimoto H. 1994. Podiform chromitites of the Tari-Misaka ultramafic complex, Southwestern Japan, as mantle–melt interaction

products. Economic Geology, 89, 1279–1288. doi: 10.2113/gsecongeo.89.6.1279.

Arai S. 1994. Characterization of spinel peridotites by olivine-spinel compositional relationships: Review and interpretation. Chemical Geology, 113, 191–204. doi: 10.1016/0009-2541(94)90066-3.

Arai S, Kadoshima K, Morishita T. 2006. Widespread arc-related melting in the mantle section of the northern Oman ophiolite as inferred from detrital chromian chromian spinels. Journal of the Geological Society, 163, 869–879. doi: 10.1144/0016-76492005-057.

Arculus RJ. 1994. Aspects of magma genesis in arcs. Lithos, 33, 1–3, 189–208. doi: 10.1016/0024-4937(94)90060-4.

Augé T. 1987. Chromite deposits in the northern Oman ophiolite: mineralogical constraints. Mineralium Deposita, 22, 1–10. doi: 10.1007/bf00204235.

Ballhaus C. 1998. Origin of podiform chromite deposits by magma mingling. Earth and Planetary Science Letters, 156, 185–193. doi: 10.1016/S0012-821X(98)00005-3.

Ballhaus C, Berry RF, Green DH. 1991. High pressure experimental calibration of the olivine–orthopyroxene–spinel oxygen barometer: implications for the oxidation state for the upper mantle. Contribution to Mineralogy and Petrology, 107, 27–40. doi: 10.1007/BF00311183.

Barnes SJ, Boyd R, Korneliussen A, Nilsson LP, Often M, Pedersen RB, Robins B. 1988. The use of mantle normalization and metal rations in discriminating between the effects of partial melting, crystal fractionation and sulphide segregation on platinum-group elements, gold, nickel and copper: examples from Norway. In: Prichard HM, Potts PJ, Bowles JFW, Cribb SJ. (eds.), Geo-Platinum Symposium Volume. Elsevier, London, 113–143. doi: 10.1007/978-94-009-1353-0_12.

Barnes SJ, Roeder PL. 2001. The range of spinel composition in terrestrial mafic and ultramafic rocks. Contribution to Mineralogy and Petrology, 42, 2279–2302. doi: 10.1093/petrology/42.12.2279.

Beccaluva L, Coltorti M, Premti I, Saccani E, Siena F, And Zeda O. 1994. Mid-ocean ridge and supra-subduction affinities in ophiolitic belts from Albania. In: Beccaluva L (Ed.), Albanian Ophiolites: State of the Art and Perspectives. Ofioliti, 19, 77–96.

Beccaluva L, Ohnenstetter D, Ohnenstetter M, Paupy A. 1984. Two magmatic series with island arc affinities within the Vourinos ophiolite. Contributions to Mineralogy and Petrology, 85, 253–271. doi: 10.1007/BF00378104.

Beinlich A, Austrheim H. 2012. In situ sequestration of atmospheric CO_2 at low temperature and surface cracking of serpentinized peridotite in mine shafts. Chemical Geology, 332-333, 32–34. doi: 10.1016/j.chemgeo.2012.09.015.

Beinlich A, Austrheim H, Mavromatis V, Grguric B, Putnis CV, Putnis A. 2018. Peridotite weathering is the missing ingredient of Earth's continental crust composition. Nature Communications, 9, 634. doi: 10.1038/S41467-018-03039-9.

Bodinier JL, Godard M. 2003. Orogenic, ophiolitic, and abyssal peridotites. In: Carlson RW (Ed.), Mantle and Core. Treatise on GeochemTreatise on Geochemistry 2. Elsevier Science Ltd., 103–170. doi: 10.1016/B978-0-08-095975-7.00204-7.

Borisova A, Ceuleneer G, Kamenetsky V, Arai S, Béjina F, Bindeman I, Polvé M, de Parseval P, Aigouy T, Pokrovski G. 2012. A new view on the petrogenesis of the Oman ophiolite chromitites from microanalyses of chromite-hosted inclusions. Journal of Petrology, 53, 2411–2440. doi: 10.1093/petrology/egs054.

Chou CL, Shaw DM, Crocket JH. 1983. Siderophile trace elements in Earth 's oceanic crust and upper mantle. Journal of Geophysical Research, 88(S2), 507–518. doi: 10.1029/JB088iS02p0A507.

Dai JG, Wang CS, Hebert R, Santosh M, Li YL, Xu JY. 2011. Petrology and geochemistry of peridotites in the Zhongba ophiolite, Yarlung Zangbo Suture Zone: Implications for the early subduction zone within the Neo–Tethys. Lithos, 288(3-4), 133–148. doi: 10.1016/j.chemgeo.2011.07.011.

Dare SAS, Pearce JA, McDonald I, Styles MT. 2009. Tectonic discrimination of peridotites using fO_2–Cr# and Ga–Ti–Fe^{III} systematic in chrome-spinel. Chemical Geology, 261, 199–216. doi: 10.1016/j.chemgeo.2008.08.002.

Dick HJ, Bullen T. 1984. Chromian magnesiochromite as a petrogenetic indicator in abyssal and Alpine-type peridotites and spatially associated lavas. Contributions to Mineralogy and Petrology, 86, 54–76. doi: 10.1007/BF00373711.

Dick HJ, Natland JH. 1996. Late-stage melt evolution and transport in the shallow mantle beneath the East Pacific Rise. Proceedings-Ocean Drilling Program Scientific Results. National Science Foundation, 103–134. doi: 10.2973/odp.proc.sr.147.007.1996.

Dilek Y, Furnes H. 2011. Ophiolite genesis and global tectonics: geochemical and tectonic fingerprinting of ancient oceanic lithosphere. Geological Society of America Bulletin, 123, 387–411. doi: 10.1130/B30446.1.

Dilek Y, Furnes H. 2014. Ophiolites and their origins. Elements, 10, 93–100. doi: 10.2113/GSELEMENTS.10.2.93.

Dilek Y, Robinson PT. 2003. Ophiolites in Earth History: Introduction, in Dilek Y, Robinson PT. (eds.), Ophiolites in Earth History. Geological Society, London, Special Publication, 218, 1–8. doi: 10.1144/GSL.SP.2003.218.01.01.

Dunkel KG, Jamtveit B, Austrheim H. 2019. Ophiocarbonates of the Feragen ultramafic body, central Norway. Norwegian Journal of Geology, 99, 1–18. doi: 10.17850/njg99-3-3.

Gervilla F, Proenza JA, Frei R, González-Jiménez JM, Garrido CJ, Melgarejo JC, Meibom A, Díaz-martínez R, Lavaut W. 2005. Distribution of platinum-group elements and Os isotopes in chromite ores from Mayarí-Baracoa ophiolilte belt (eastern Cuba). Contributions to Mineralogy and Petrology, 150, 589–607. doi: 10.1007/s00410-005-0039-2.

Ghiorso MS, Hirschmann MM, Reiners PW, Kress III VC. 2002. The pMELTS: a revision of MELTS aimed at improving calculation of phase relations and major element partitioning involved in partial melting of the mantle at pressures up to 3 GPa. Geochemistry Geophysics Geosystems, 3 (5). doi: 10.1029/2001GC000217.

Godard M, Jousselin D, Bodinier JL. 2000. Relationships between geochemistry and structure beneath a palaeo-spreading centre: a study of the mantle section in the Oman ophiolite. Earth and Planetary Science Letters, 180, 133–148. doi: 10.1016/S0012-821X(00)00149-7.

Hamlyn PR, Keays RR, Cameron WE, Crawford AJ, Waldron HM. 1985. Precious metals in magnesian low-Ti lavas: implications for metallogenesis and sulfur saturation in primary magmas. Geochimica et Cosmochimica Acta, 49, 1797–1811. doi: 10.1016/0016-7037(85)90150-4.

Jackson SE, Fryer BJ, Gosse W, Healey DC, Longerich HP, Strong DF. 1990. Determination of the precious metals in geological materials by inductively coupled plasma-mass spectrometry (ICP-MS) with nickel sulphide fire-assay collection and tellurium coprecipitation. Chemical Geology, 83(1–2), 119–132. doi: 10.1016/0009-2541(90)90144-V.

Kamenetsky VS, Crawford AJ, Meffre S. 2001. Factors controlling chemistry of magmatic magnesiochromite: an empirical study of associated olivine, Cr-magnesiochromite and melt inclusions from primitive rocks. Journal of Petrology, 42, 655–671. doi: 10.1093/petrology/42.4.655.

Li JQ, Zhang YS, Li X, Ren SS, Ran LN. 2023. Identification of clayey altered ophiolite in the Nujiang tectonic belt and new understanding of its impacts on engineering stability. China Geology, 6(4), 756–758. doi: 10.31035/cg2023076.

Maurel C, Maurel P. 1982. Experimental study of the solubility of chromium in mafic silicate baths and its partitioning between liquid and coexisting minerals: conditions of existence of chromian magnesiochromite. Bulletin de minéralogie, 105, 640–647.

McDonough WF, Sun SS. 1995. The composition of the Earth. Chemical Geology, 120(3), 223–254. doi: 10.1016/0009-2541(94)00140-4.

Melcher F, Grum W, Thalhammer T, Thalhammer O. 1999. The giant chromite deposits at Kempirsai, Urals: constraints from trace element (PGE, REE) and isotope data. Mineralium Deposita, 34, 250–272. doi: 10.1007/s001260050202.

Miller C, Thöni M, Frank W, Schuster R, Melcher F, Meisel T, Zanetti A. 2003. Geochemistry and tectonomagmatic affinity of the Yungbwa ophiolite, SW Tibet. Lithos, 66, 155–172. doi: 10.1016/S0024-4937(02)00217-7.

Moore AC, Hultin I. 1980. Petrology, mineralogy, and origin of the Feragen ultramafic body, Sør-Trøndelag, Norway. Norsk Geologisk Tidsskrift, 60, 235–254. doi: 10.1007/978-94-009-8117-1.

Moores EM. 1982. Origin and emplacement of ophiolites. Reviews of Geophysics, 20, 735–760. doi: 10.1029/RG020i004p00735.

Nakamura M. 1995. Residence time and crystallization history of nickeliferous olivine phenocrysts from the northern Yatsugatake volcanoes, Central Japan: application of a growth and diffusion model in the system Mg-Fe-Ni. Journal of Volcanology and Geothermal Research, 66, 81–100. doi: 10.1016/0377-0273(94)00054-K.

Nilsson LP, Roberts D. 2014. A trail of ophiolitic debris and its detritus along the Trøndelag-Jämtland border: correlations and palaeogreographical implications. Norges Geologiske undersø kelse Bulletin, 453, 29–41.

Nilsson LP, Roberts D, Ramsay DM. 2005. Te Raudfellet ophiolite fragment, Central Norwegian Caledonides: pricipal lithological and structural features. Norges Geologiske undersø kelse Bulletin, 445, 101–117.

Nilsson LP, Sturt BA, Ramsay DM. 1997. Ophiolitic ultramaftes in the Folldal-Røros tract, and their Cr-(PGE) mineralization (Extended abstract). Norges Geologiske undersø kelse Bulletin, 433, 10–11.

Niu Y. 2004. Bulk-rock major and trace element compositions of abyssal peridotites: Implications for mantle melting, melt extraction and post-melting processes beneath mid-ocean ridges. Journal of Petrology, 45, 2423–2458. doi: 10.1093/petrology/egh068.

Niu Y, Langmuir CH, Kinzler RJ. 1997. The origin of abyssal peridotites: a new perspective. Earth and Planetary Science Letters, 152(1), 251–265. doi: 10.1016/S0012-821X(97)00119-2.

O 'Neill H, Wall V. 1987. The olivine–orthopyroxene–spinel oxygen geobarometer, the nickel precipitation curve and the oxygen fugacity of the earth upper mantle. Journal of Petrology, 28, 169–1191. doi: 10.1093/petrology/28.6.1169.

Ozawa K. 1994. Melting and melt segregation in the mantle wedge above a subduction zone: evidence from the chromite-bearing peridotites of the Miyamori Ophiolite Complex, northeastern Japan. Journal of Petrology, 35, 647–678. doi: 10.1093/petrology/35.3.647.

Pagé P, Barnes SJ. 2009. Using trace elements in chromites to constrain the origin of podiform chromitites in the Thetford mines ophiolite, Québec, Canada. Economic Geology, 104, 997–1018. doi: 10.2113/econgeo.104.7.997.

Pagé P, Bédard JH, Schroetter JM, Tremblay A. 2008. Mantle petrology and mineralogy of the Thetford Mines ophiolite complex. Lithos, 100, 255–292. doi: 10.1016/j.lithos.2007.06.017.

Palme H, O 'Neill HSC. 2004. Cosmochemical estimates of mantle composition. In:Holland HD, TurrekianKK.(eds.), –38. doi: 10.1016/B0-08-043751-6/02177-0.

Parkinson IJ, Arculus RJ. 1999. The redox state of subduction zones: insights from arc-peridotites. Chemical Geology, 160, 409–423. doi: 10.1016/s0009-2541(99)00110-2.

Parkinson IJ, Pearce JA. 1998, Peridotites from the Izu-Bonin-Mariana forearc (ODP Leg 125): evidence for mantle melting and melt-mantle interaction in a supra-subduction zone setting. Journal of Petrology, 39, 1577–1618. doi: 10.1093/petroj/39.9.1577.

Pearce JA, Barker PF, Edwards SJ, Parkinson IJ, Leat PT. 2000. Geochemistry and tectonic significance of peridotites from the South Sandwich arc-basin system, South Atlantic. Contributions to Mineralogy and Petrology, 139, 36–53. doi: 10.1007/s004100050572.

Pearce JA, Lippard SJ, Roberts S. 1984. Characteristics and tectonic significance of supra-subduction zone ophiolites. In: Kokelaar BP, Howells MF. (eds.), Marginal Basin Geology. Geological Society of London Special Publication, 16, 77–89. doi: 10.1144/GSL.SP.1984.016.01.06.

Qiao GB, Li WM, Li TH. 2023. SHRIMP zircon U-Pb age and O isotopic analysis of the dunite from Kudi ophiolite in the West Kunlun, China. China Geology, 6(1), 171–173. doi: 10.31035/cg2021047.

Roberts D. 1974. Sedimentary, tectonic and metamorphic features of the Devonian of Røragen, Sør-Trøndelag. Norges Geologiske undersø kelse Bulletin, 311, 89–108.

Robinson PT, Trumbull RB, Schmitt A, Yang JS, Li JW, Zhou MF, Erzinger J, Dare S, Xiong FH. 2015. The origin and significance of crustal minerals in ophiolitic chromitites and peridotites. Gondwana Research, 27, 486–506. doi: 10.1016/j.gr.2014.06.003.

Rollinson H. 2008. The geochemistry of mantle chromitites from the northern part of the Oman ophiolite: inferred parental melt compositions. Contributions to Mineralogy and Petrology, 156, 273–288. doi: 10.1007/s00410-008-0284-2.

Sack RO, Ghiosro MS. 1991. Chromian spinel as petrogenetic indicators: thermodynamics and petrological applications. American Mineralogist, 76, 827–847. doi: 10.1180/minmag.1991.055.379.18.

Shervais JW. 2001. Birth, death, and resurrection: the life cycle of suprasubduction zone ophiolites. Geochemistry, Geophysics, Geosystems, 2(1), 148–159. doi: 10.1029/2000GC000080.

Smith SE, Elthon D. 1988. Mineral compositions of plutonic rocks from the Lewis Hills massif, Bay of Islands ophiolite. Journal of Geophysical research, 93, 3450–3468. doi: 10.1029/JB093iB04p03450.

Sun M, Jain J, Zhou M, Kerrich R. 1993. A procedural modification for enhanced recovery of precious metals (Au, PGE) following nickel sulphide fire assay and tellurium co-precipitation: applications for analysis of geological samples by inductively coupled plasma mass spectrometry. Canadian journal of applied spectroscopy, 38, 103–108.

Sun Y, Sun M. 2005. Nickel sulfide fire assay improved for pre-concentration of platinum-group elements in geological samples: a practical means of ultra-trace analysis combined with inductively coupled plasma-mass spectrometry. Analyst, 130, 664–669. doi: 10.1039/b416844e.

Ulven IO, Hovelmann J, Austrheim H, Jamtveit B, Beinlich A. 2017. Subarctic physiochemical weathering of serpentinized peridotite. Earth and Planetary Science Letters, 486, 11–26. doi: 10.1016/j.epsl.2017.03.030.

Uysal I, Akmaz RM, Kapsiotis A, Demir Y, Saka S, Avcı E, Müller D. 2015. Genesis and geodynamic significance of chromitites from the Orhaneli and Harmancık ophiolites (Bursa, NW Turkey) as evidenced by mineralogical and compositional data. Ore Geology Reviews, 65, 26–41. doi: 10.1016/j.oregeorev.2014.08.006.

Uysal I, Sadiklar M, Tarkian M, Karsli O, Aydin F. 2005. Mineralogy and composition of the chromitites and their platinum-group minerals from Ortaca (Muğla-SW Turkey): evidence for ophiolitic chromitite genesis. Mineralogy and Petrology, 83, 219–242. doi: 10.1007/s00710-004-0063-3.

Uysal I, Tarkian M, Sadiklar MB, Zaccarini F, Meisel T, Garuti G,

Heidrich S. 2009. Petrology of Al- and Cr-rich ophiolitic chromitites from the Mugla, SW Turkey: implications from composition of chromite, solid inclusions of platinum-group mineral, silicate, and base-metal mineral, and Os-Isotope geochemistry. Contributions to Mineralogy and Petrology, 158, 659–674. doi: 10.1007/s00410-009-0402-9.

Uysal IM, Kaliwoda M, Karsli O, Tarkian M, Sadiklar MB, Ottley CJ. 2007. Compositional variations as a result of partial melting and melt–peridotite interaction in an upper mantle section from the Ortaca area, southwestern Turkey. The Canadian Mineralogist, 45, 1471–1493. doi: 10.3749/canmin.45.6.1471.

Wan Z, Laurence A, Coogan LA, Canil D. 2008. Experimental calibration of aluminum partitioning between olivine and spinel as a geothermometer. American Mineralogist, 93, 1142–1147. doi: 10.2138/am.2008.2758.

Wilson M. 1989. Igneous Petrogenesis. Unwin Hyman, London. pp 446.

Xiong FH, Basem Z, Xu XZ, Davide L, Yang JS. 2022. Genesis and high-pressure evolution of the Koycegiz ophiolite (SW Turkey): mineralogical and geochemical characteristics of podiform chromitites. Ore Geology Reviews, 145, 104912. doi: 10.1016/j.oregeorev.2022.104912.

Xiong FH, Yang JS, Robinson PT, Xu XZ, Liu Z, Li Y, Li JY, Chen SY. 2015. Origin of podiform chromitite, a new model based on the Luobusa ophiolite, Tibet. Gondwana Research, 27(2), 525–542. doi: 10.1016/j.gr.2014.04.008.

Yamamoto S, Komiya T, Hirose K, Maruyama S. 2009. Coesite and clinopyroxene exsolution lamellae in chromites: In-situ ultrahigh-pressure evidence from podiform chromitites in the Luobusa ophiolite, southern Tibet. Lithos, 109, 314–322. doi: 10.1016/j.lithos.2008.05.003.

Yang JS, Robinson PT, Dilek Y. 2014. Diamonds in ophiolites. Elements, 10, 127–130. doi: 10.2113/gselements.10.2.127.

Yang JS, Robinson PT, Xu X, Dilek Y. 2013. Ophiolite-type diamond: a new occurrence of diamond on the Earth. EGU General Assembly Conference Abstracts, 13613.

Zhou MF, Robinson PT, Bai WJ. 1994. Formation of podiform chromitites by melt/rock interaction in the upper mantle. Mineralium Deposita 29(1), 98–101. doi: 10.1007/BF03326400.

Zhou MF, Robinson PT, Malpas J, Li ZJ. 1996. Podiform chromitites in the Luobusa ophiolite (southern Tibet): Implications for melt-rock interaction and chromite segregation in the upper mantle. Journal of Petrology, 37, 3–21. doi: 10.1093/petrology/37.1.3.

Zhou MF, Robinson PT, Malpas J, Edwards SJ, Qi L. 2005. REE and PGE geochemical constraints on the formation of dunites in the Luobusa ophiolite, southern Tibet. Journal of Petrology, 46, 615–639. doi: 10.1093/petrology/egh091.

Zhou MF, Robinson PT, Su BX, Gao JF, Li JW, Yang JS, Malpas J. 2014. Compositions of chromite, associated minerals, and parental magmas of podiform chromite deposits: the role of slab contamination of asthenospheric melts in suprasubduction zone environments. Gondwana Research, 26(1), 262–283. doi: 10.1016/j.gr.2013.12.011.

Zhou MF, Sun M, Keays RR, Kerrich RW. 1998. Controls on platinum-group elemental distributions of podiform chromitites: a case study of high-Cr and high-Al chromitites from Chinese orogenic belts. Geochimica et Cosmochimica Acta, 62, 677–688. doi: 10.1016/S0016-7037(97)00382-7.